Towards robust sequential ultrasonic spot welding of thermoplastic composites: Welding process control strategy for consistent weld quality

Tian Zhao*, Charlotte Broek, Genevieve Palardy, Irene Fernandez Villegas and Rinze Benedictus

Structural Integrity and Composites Group, Faculty of Aerospace Engineering, Delft University of Technology, Kluyverweg 1, 2629HS, Delft, The Netherlands

Corresponding author: T.Zhao@tudelft.nl

Abstract

The research presented in this paper is an essential part of a bigger effort on developing robust sequential ultrasonic welding of multi-spot welded joints in thermoplastic composites. It mainly focused on assessing the impact of the changes in boundary conditions on the welding process and whether it could be circumvented by using an appropriate process control strategy. A two-step approach was followed by investigating: (1) the effect of boundary conditions on displacement- and energy-controlled single-spot welded joints and (2) displacement- and energy-controlled sequential ultrasonic welding of double-spot welded joints. The results showed that previous spots indeed affect the welding energy required to obtain an optimum new welded spot, which challenges the use of energy-controlled welding for this application. Contrarily, displacement-controlled welding was shown to provide consistent-quality welds with a constant set of welding parameters and it was hence identified as the most promising welding strategy for sequential ultrasonic welding of thermoplastic composite structures.

Keywords: **Thermoplastic resin, Mechanical properties, Fractography, Joints/joining**

Introduction

Ultrasonic welding is an attractive joining technique for thermoplastic composites (TPCs), owing to the short welding times, absence of foreign materials at the weldline, possibility for in-situ monitoring and ease of automation [1-3]. However, upscaling of the ultrasonic welding process for assemblies with large overlaps is still a challenge [4]. Ultrasonic welding is by nature a spot welding technique, hence the most straightforward upscaling route is sequential welding of consecutive spots resulting in a multi-spot welded (MSW) joint. According to our previous research [5], single-spot welded (SSW) thermoplastic composite joints feature similar shear strength to joints with a single mechanical fastener of comparable size. Consequently, multi-spot sequential welding has the potential to become a composite-friendly and fast-processing plausible alternative to mechanical fastening in thermoplastic composite structures.

Unlike ultrasonic spot welding of metallic materials [6-9], ultrasonic spot welding of thermoplastic composites has been barely explored. In the early 90's, Lu and Benatar [10] reported successful results on sequential ultrasonic welding of thermoplastic composites however they provided no details on the way the process was carried out. To the best of the authors' knowledge, little to no research on the topic has been reported in the open literature since then. One of the main challenges of sequential ultrasonic welding is the fact that the boundary conditions of the welding process are likely to change with each new welded spot. In particular, the number of welded spots affects the boundary conditions for each new welded spot (see Fig. 1)

and hence is expected to influence the way in which the ultrasonic vibration is distributed among the welding interface, the adherends and the welding jig. Consequently, obtaining welded spots of consistent quality in a sequential MSW joint might require that different welding parameters are used for each spot if the welding process is not adequately controlled.

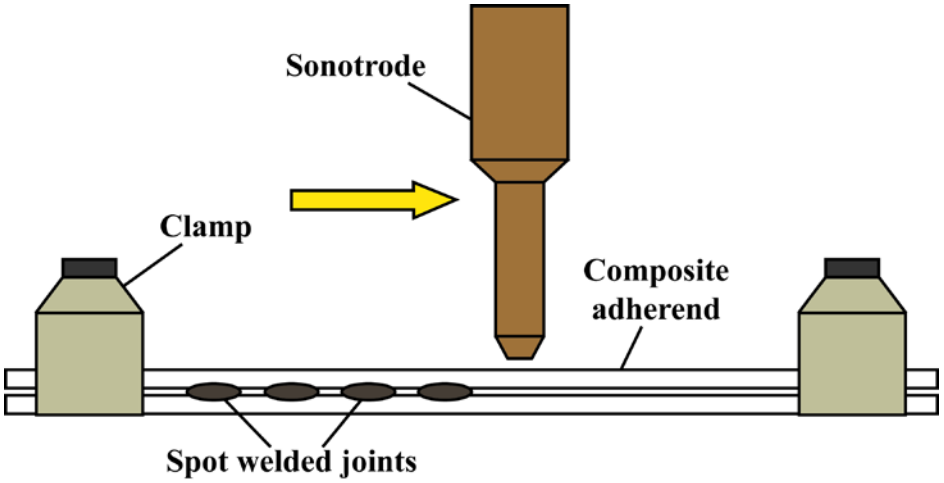

Fig. 1. Schematic of the sequential ultrasonic spot welding process. The welds already created introduce new boundary conditions for each new spot to be welded.

Microprocessor-controlled ultrasonic welders allow different modes to directly or indirectly control the duration of the vibration phase in the process. These control modes are typically based on the vibration time, the consumed energy or the vertical displacement of the sonotrode. Among these, energy and displacement (i.e. indirect) control are typically preferred over time (i.e. direct) control. Harras *et al.* [11] performed a comparative study between time and energy control modes for the single-step ultrasonic welding of Mode I and Mode II fracture toughness of carbon fibre reinforced polyetheretherketone (CF/PEEK) samples. Their results showed that

the maximum critical strain energy release rates (G_{IC} and G_{IIC}) were obtained when a constant welding energy input was used. However, the optimum welding time (i.e. the welding time resulting in maximum G_{IC} and G_{IIC}) was found to depend significantly on the sample configuration. Similarly, different research [12] showed a good correlation between weld strength and input weld energy for samples with different surface roughness. Finally, energy-controlled ultrasonic welding was successfully used in our previous research [5] to manufacture SSW joints in CF/PEEK adherends with consistent strength, failure modes and welded surface area. Despite these successful results for energy-controlled welding, it must be noted that the welding energy is not only invested in creating the welded joints but it is also dissipated in the adherends and in the clamping jig [13]. Hence, changes in e.g. the thickness or stiffness of the adherends do have a significant impact in the energy required for the welding process [2]. Consequently, the changing boundary conditions in sequential ultrasonic welding can be expected to affect the energy required to weld each spot.

Alternatively, displacement-controlled welding, in which the duration of the vibration phase is indirectly controlled through the vertical displacement of the sonotrode, has provided promising results for single-step ultrasonic welding of single-lap shear samples [2]. In particular, the vertical displacement of the sonotrode during the ultrasonic welding process can be directly related to the physical changes occurring at the weldline and the uppermost layer of the adherends. Moreover, it is relatively independent of the energy dissipated in the surroundings and has hence the potential to be insensitive to the changing boundary conditions during sequential ultrasonic welding of MSW joints.

The research presented in this paper is geared towards the development of sequential ultrasonic welding of multi-spot welded joints in thermoplastic composite structures. As previously mentioned, in sequential ultrasonic welding of MSW joints, each welded spot will introduce changes in the boundary conditions for the new spot to be welded. Our hypothesis is that these changes will affect the welding energy required to obtain optimum weld quality but will not affect the displacement required to obtain optimum weld quality in a displacement-controlled welding process. In order to test this hypothesis, a two-step approach was followed in this research. Firstly, the effect of changing boundary conditions on the quality of single-spot welded joints obtained via displacement- and energy-controlled welding was investigated. Changes in the boundary conditions were introduced through the usage of two different clamping jigs. Secondly, double-spot welded joints were investigated to assess the effect of the existence of a first welded spot on the quality of the second welded spot based on the knowledge gained in the first part of the research. Both displacement- and energy-controlled double-spot welded joints were also investigated in this second part. In both parts, the quality of the welded joints was assessed through single-lap shear testing, fractography and measurement of the welded area. When required, additional information about the welding processes was obtained through the feedback data, i.e. power and sonotrode displacement, provided by the ultrasonic welder.

2 Experimental

2.1 Materials

The thermoplastic composite material used in this study was 5 harness satin fabric carbon fibre reinforced polyphenylene sulphide (CF/PPS) supplied by Ten Cate Advanced Composites, The Netherlands. Laminates, consisting of six semi-impregnated fabric layers in a $[0/90]_{3s}$ stacking sequence, were consolidated in a hot platen press at 320 °C and 1 MPa for 20 min. The resulting laminates had a final nominal thickness of 1.62 mm and 58 % nominal fibre volume fraction. Rectangular adherends were cut from these laminates with a water-cooled diamond saw with their longitudinal direction parallel to the main orientation of the fibres on the surface of the laminate. In the case of the single-spot welded (SSW) joints, the dimensions of the adherends were 101.6 x 25.4 mm^2 and they were spot welded in the centre of a 25.4 x 25.4 mm^2 overlap, as shown in Fig. 2a. In the case of the double-spot welded (DSW) joints, the dimensions of the adherends were 120 x 25.4 mm^2 and two spots were welded in a 50 x 25.4 mm^2 overlap. The distance between the centres of the welded spots was 20 mm (see Fig. 2b).

Spot, i.e. circular, 4 mm-diameter energy directors (EDs) were used in this study. These were cut from flat ED films with a nominal thickness of approximately 0.25 mm obtained from three 0.08 mm-thick neat PPS films consolidated in a hot platen press at 260 °C and 2 MPa for 10 min. The spot EDs were manually fixed on the bottom adherend with a Rinco handheld ultrasonic welder prior to the welding process. The position of the EDs in the overlap for both the SSW and the DSW joints is also shown in Fig. 2.

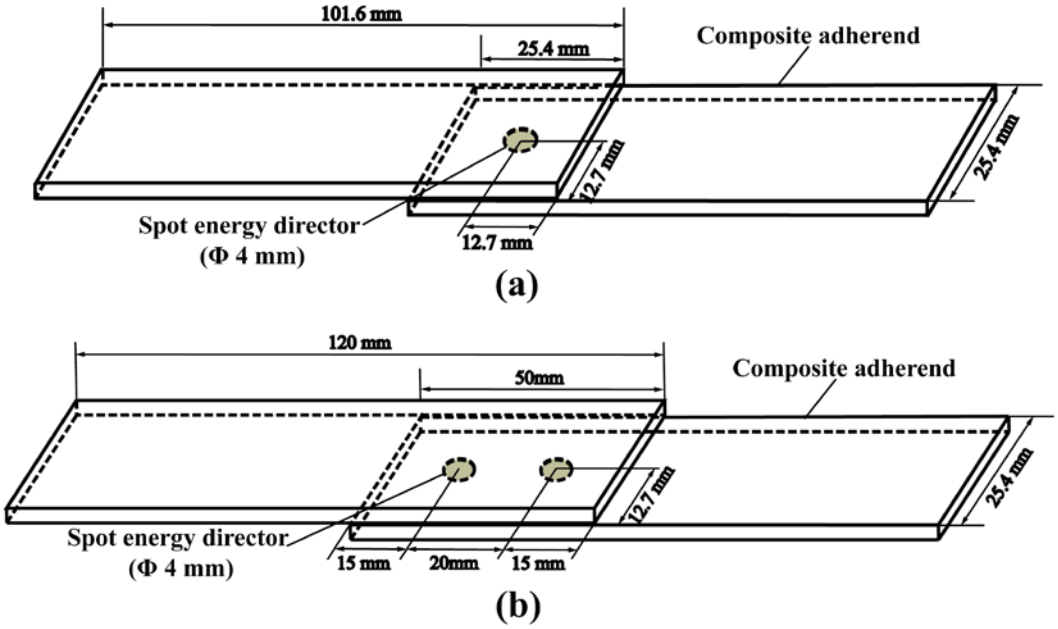

Fig. 2. Schematic of (a) the single-spot welded joints and (b) the double-spot welded joints used in this study. The grey dashed ellipses indicate the locations of the spot energy directors. Dimensions are not to scale.

2.2 Ultrasonic welding process

A 20 kHz Rinco Dynamic 3000 microprocessor-controlled ultrasonic welder with a 10 mm-diameter circular titanium sonotrode (see Fig. 3) was used to produce the spot welds in this research. For the first part of the study, two different custom-designed welding jigs, hereafter referred to as Jig 1 (Fig. 3a) and Jig 2 (Fig. 3b), were used to produce SSW joints with different boundary conditions. Jig 1 featured the most simple and flexible configuration with two bars used to clamp the adherends away from the welding overlap. In this jig, the top adherend partially rested on the bottom adherend and on a 1.5 mm-thick aluminium base plate, as schematically shown in Fig. 4a. This configuration introduced a small misalignment between the surfaces of the adherends which was corrected once the sonotrode applied pressure on the overlap. This thin base plate nevertheless allowed for unobstructed downward

movement of the sonotrode during melting and flow of the ED. In Jig 2, the top adherend was clamped onto a platform supported by four springs and parallel to the base of the jig (see Fig. 4b). It must be noted that, owing to the fact that in Jig 2, the adherends were nominally parallel to each other throughout the welding process, the ED could be expected to undergo more uniform strains than in the case of Jig 1. In the second part of the study, Jig 1 was used to produce the DSW joints. In these joints, the first spot was welded and subsequently, the sample was manually shifted to weld the second spot. The order in which the two spots were sequentially welded in the DSW joints is indicated in Fig. 5. Owing to the small contact surface of the sonotrode (10 mm diameter) and the small surface of the EDs (4 mm diameter) as compared to the distance between spots (20 mm centre-to-centre distance) there was virtually no interaction between the first and the second weld in the DSW joints. Consequently the two welding processes necessary to create the DSW joints had the same characteristics (i.e. heating and melting of a pristine ED followed by squeeze flow and downward displacement of the top adherend) as the welding process in each SSW joint, as it will be shown in section 4 of this paper.

During the vibration phase of the welding process, a mechanical vibration with 60.8 μm peak-to-peak amplitude was introduced in the welding stack. The welding force at the onset of the vibration phase was 1500 N and it was linearly increased at a rate of 1000 N/s throughout the vibration phase. Subsequently, the welded joint was cooled down under 1500 N force for 4 s. Either the vertical displacement of the sonotrode or the welding energy was used to indirectly control the duration of the vibration phase in displacement-controlled and energy-controlled welding,

respectively. That is to say, the vibration phase was automatically stopped when either the pre-defined sonotrode vertical displacement or the consumed energy value was reached.

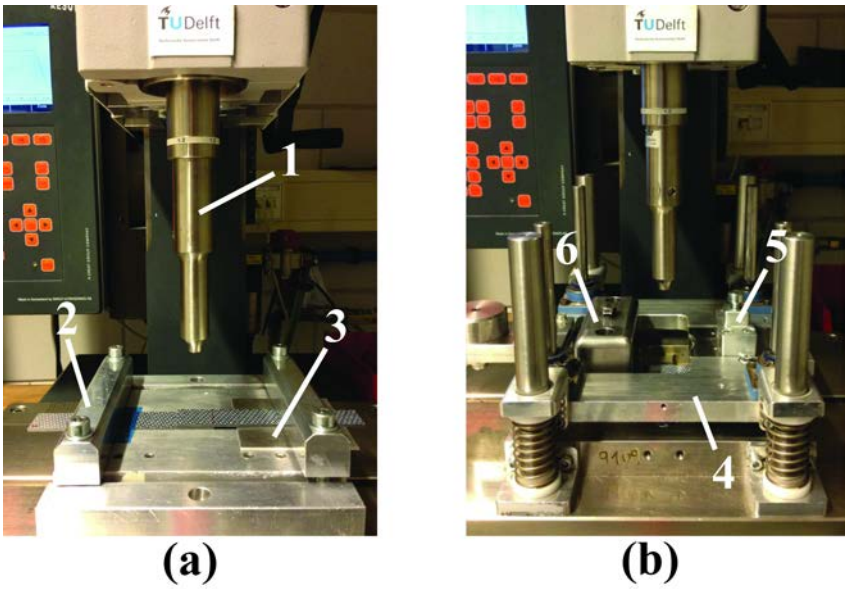

Fig. 3. Ultrasonic welder, circular sonotrode and welding jigs used in this study: (a) Jig 1 and (b) Jig 2. 1. sonotrode, 2: bar clamp in Jig 1, 3: supporting plate, 4: sliding platform in Jig 2, 5: clamp for the top adherend and 6: clamp for the bottom adherend. (For interpretation of the references to colour in this figure legend, the reader is referred to the web version of this article.)

Following the procedure explained in [2], the optimum displacement (displacement-controlled welding process) or the optimum welding energy (energy-controlled welding process) was determined using the power and displacement curves provided by the ultrasonic welder. As described in detail in [2, 3], based on power and displacement data, the vibration phase of the welding process can be divided in the five stages depicted in Fig. 6. These stages are related to the physical changes undergone by the ED and adherends and ultimately to the weld strength [2]. Therefore, the power and displacement curves can be used to determine the optimum

displacement or the optimum welding energy, i.e. the displacement or energy values that result in maximised weld strength. These have been shown to lie within stage 4, which coincides with the occurrence of a second power peak or plateau (see Fig. 6) [2, 3]. In the first part of this study, optimum displacement and energy values were identified for the SSW joints in Jigs 1 and 2. Subsequently, the optimum displacement and energy values for the SSW joints in Jig 1 were used to weld the DSW joints in the second part of this study.

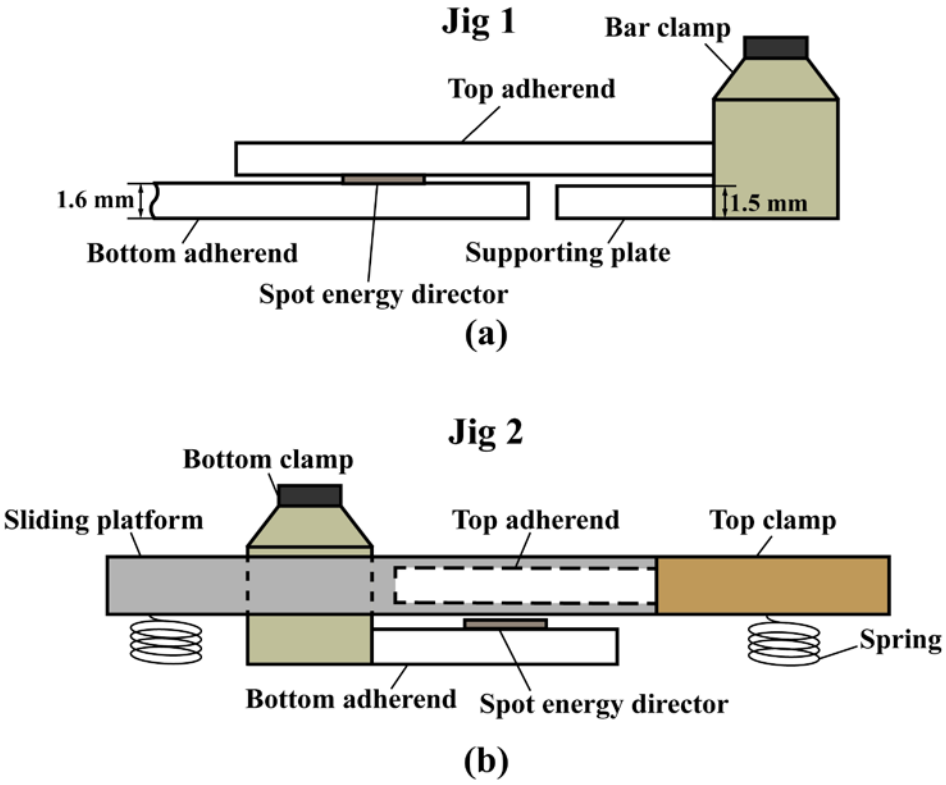

Fig. 4. Schematic of the clamping situation for the SSW joints in (a) Jig 1 and (b) Jig 2. Dimensions are not to scale. (For interpretation of the references to colour in this figure legend, the reader is referred to the web version of this article.)

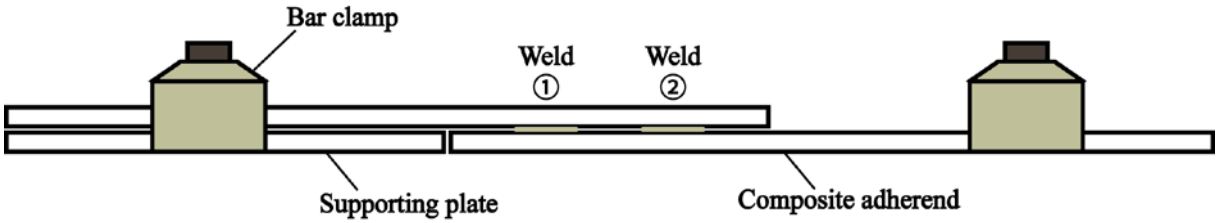

Fig. 5. Schematic of the sequence followed for the sequential welding of the DSW joints with Jig 1. "Weld 1" and "Weld 2" refer to the spot welded in the first and in the second place, respectively.

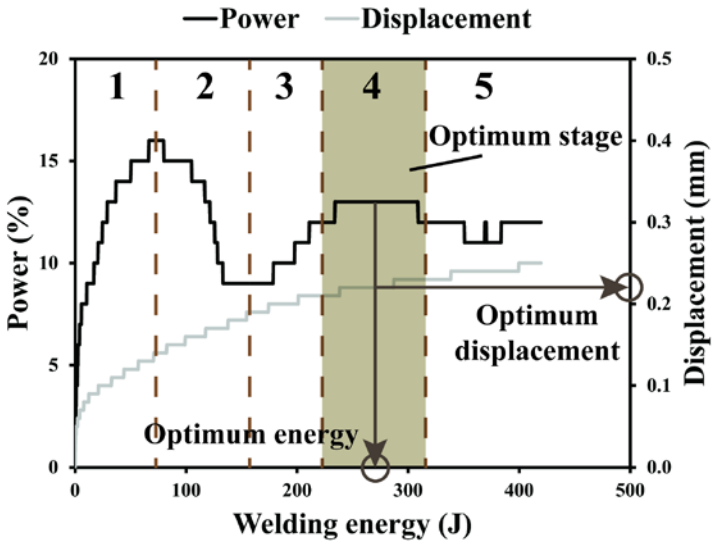

Fig. 6. Typical calibration power curve for ultrasonic spot welding process. As stated in [2], the entire welding process can be divided into 5 stages and the stage 4 is regarded as the optimum stage.

2.3 Testing and analysis

The single-lap SSW and DSW joints were mechanically tested in a Zwick/Roell 250 kN universal testing machine following the ASTM D1002 standard. The hydraulic grips of the testing machine were offset to ensure parallelism between the load path and the weldline in every sample. The distance between grips was 60 mm for the SSW samples and 85 mm for the DSW samples. Tests were initiated with a preload of approximately 100 N and performed at a crosshead speed of 1.3 mm/min. Five

samples were tested per set of welding conditions. The load-displacement response of the SSW and the DSW joints exhibited a linear behaviour and hence, the maximum load reached in the lap-shear tests, referred to as ultimate failure load (UFL), was an indicator of the load-carrying capability of the spot welded joints. After mechanical testing, the welded area (WA) in each welded spot was visually inspected via a Zeiss stereo-microscope and was measured using ImageJ150 (NIH). Fig. 7 illustrates the procedure used to define the WA of a welded spot. It must be noted that, as a general rule in this study, the flow front of the ED was not considered for the measurement of the welded area, i.e. only the area that showed failure in the composite was considered as welded area. Owing to the fact that adhesive failure was observed at the flow front, its contribution to the total weld strength was considered negligible. The UFL and WA of the SSW and DSW joints were used to gain insight into the influence of the process control on the variability of weld quality. Fractography was used to evaluate the failure mechanisms of the welded joints by using a high-resolution Zeiss stereo-microscope and a JEOL JSM-7500F scanning electronic microscope (SEM).

3 SSW joints: results and discussion

3.1 Optimum displacement/energy values

The curves in Fig. 8a and Fig. 8b show the evolution of the power and of the vertical displacement of the sonotrode as a function of the welding energy during the calibration welding process, i.e. process used to obtain optimum displacement and energy values, in Jig 1 and Jig 2, respectively. It must be noted that according to the procedure proposed in [2], the calibration samples were welded using displacement

control with a maximum nominal displacement equal to the initial thickness of the ED (i.e. 0.25 mm). As the sonotrode displacement in the welding process is a combination of displacement caused by squeeze-flow of the melted ED and deformation of both ED and adherends under the applied pressure, this maximum displacement value could be achieved. Figs. 8a and 8b also show how stage 4 was defined and how the optimum energy and displacement values were taken from around the middle of this stage. This resulted in an optimum sonotrode displacement of 0.23 mm and optimum welding energy of 420 J for Jig 1 (Fig. 8a), and optimum sonotrode displacement of 0.23 mm and optimum welding energy of 350 J for Jig 2 (Fig. 8b). Table 1 summarises the optimum welding parameters for each jig. It must be noted that even though the power curves in Figs. 8a and 8b did not show a very distinct onset or ending of stage 4, the validity of the optimum values shown in Table 1 was further proven by the results shown hereafter.

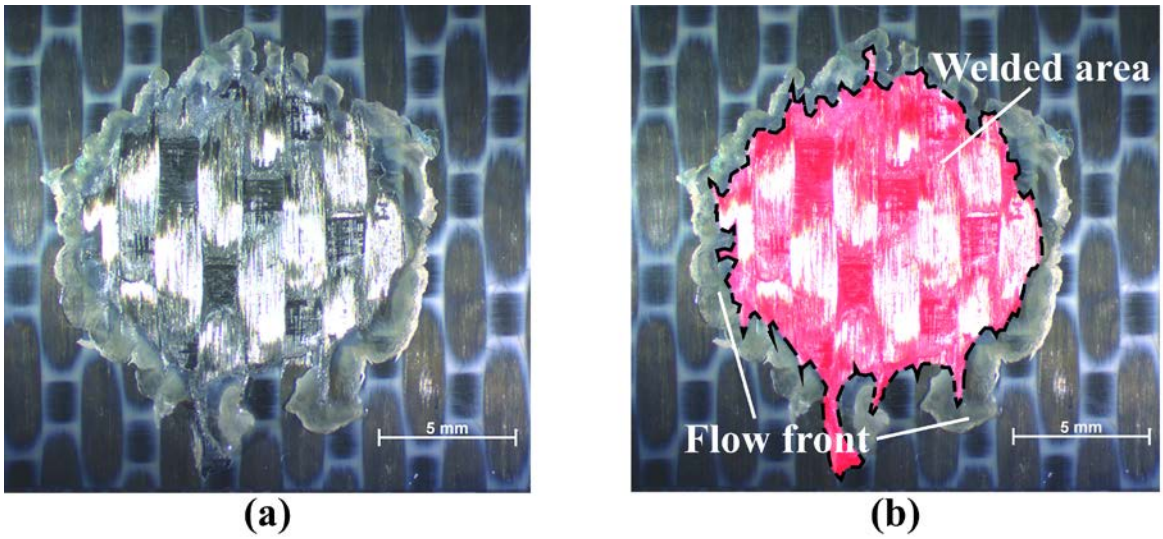

Fig. 7. (a) Representative fracture surface of SSW joint and (b) definition of the corresponding WA (delimited by the dashed line) without taking into account the flow front of the ED. (For interpretation of the references to colour in this figure legend, the reader is referred to the web version of this article.)

According to the values in Table 1, the optimum displacement seemed to be practically insensitive to the type of welding jig used whereas the optimum welding energy seemed to be significantly affected by the welding jig. In fact Jig 1, which imposed the highest constraints to the movement of the top adherend, was found to require a considerably higher welding energy than Jig 2 (around 20 % higher).

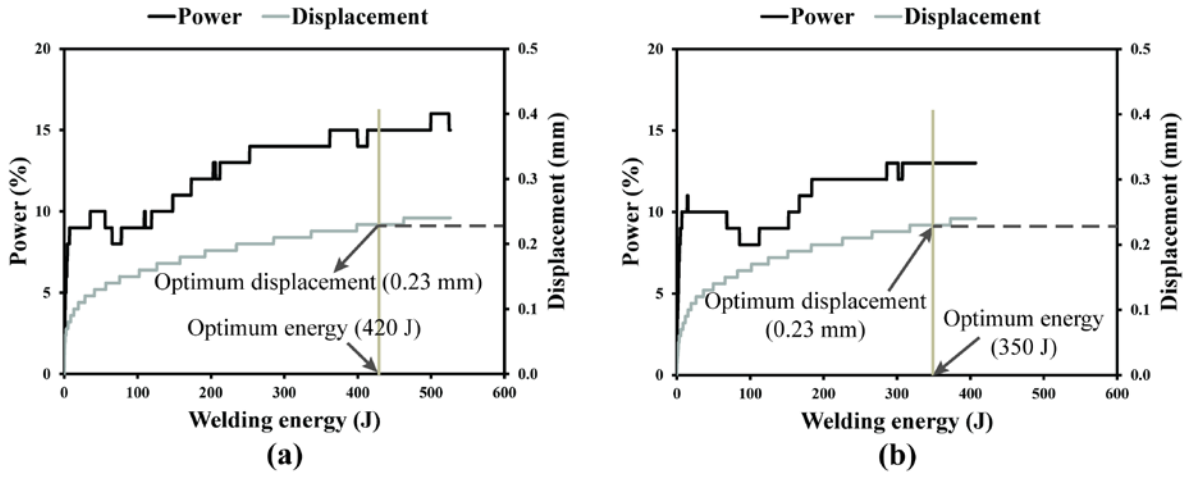

Fig. 8. Calibration power and displacement curves for displacement-controlled SSW joints obtained in (a) Jig 1 and (b) Jig 2 (60.8 µm peak-to-peak amplitude, 1500 N welding force and 1000 N/s force ramp during the vibration phase, 0.25 mm maximum displacement).

Table 1. Welding jigs, welding processes and optimum displacement/energy for the SSW joints studied in this research. Welding amplitude was 60.8 µm (peak-to-peak), initial welding force was 1500 N and welding force ramp was 1000N/s in all cases.

Weld Reference	Welding Jig	Welding Process	Optimum Displacement (mm)	Optimum Energy (J)
SSW-J1/D_{opt}	Jig 1	Displacement-controlled	0.23	-
SSW-J1/E_{opt}	Jig 1	Energy-controlled	-	420
SSW-J2/D_{opt}	Jig 2	Displacement-controlled	0.23	-
SSW-J2/E_{opt}	Jig 2	Energy-controlled	-	350

Moreover, in the power curves for the samples welded in displacement-control mode and under the optimum sonotrode displacement (0.23 mm), the vibration was found to almost consistently stop within the optimum stage of the process, i.e. stage 4

(see Fig. 9a for J1/D_{opt} and Fig. 9b for J2/D_{opt}). In the case of energy-controlled welding under optimum welding energy (i.e. 420 J for Jig1 and 350 J for Jig 2), the power curves showed that for most samples, the vibration stopped within stage 4 but they displayed more variability than in displacement-controlled welding (see Fig. 10a for J1/E_{opt} and Fig. 10b for J2/E_{opt}). This is in line with our previous observations concerning the effect of sample-to-sample variability on the optimum welding energy [2]. Despite this variability, using the optimum welding energy in energy-controlled welding still proved to result in a larger number of samples in the optimum welding stage than welding in non-optimum conditions. As shown in Fig. 11a, samples welded in Jig 1 with the optimum energy for Jig 2 (i.e. 350 J, hence lower than the optimum energy for Jig 1) did not reach the optimum welding stage. Likewise, samples welded in Jig 2 with the optimum energy for Jig 1 (i.e. 420 J, hence higher than the optimum energy for Jig 2) went beyond the optimum welding stage (see Fig. 11b).

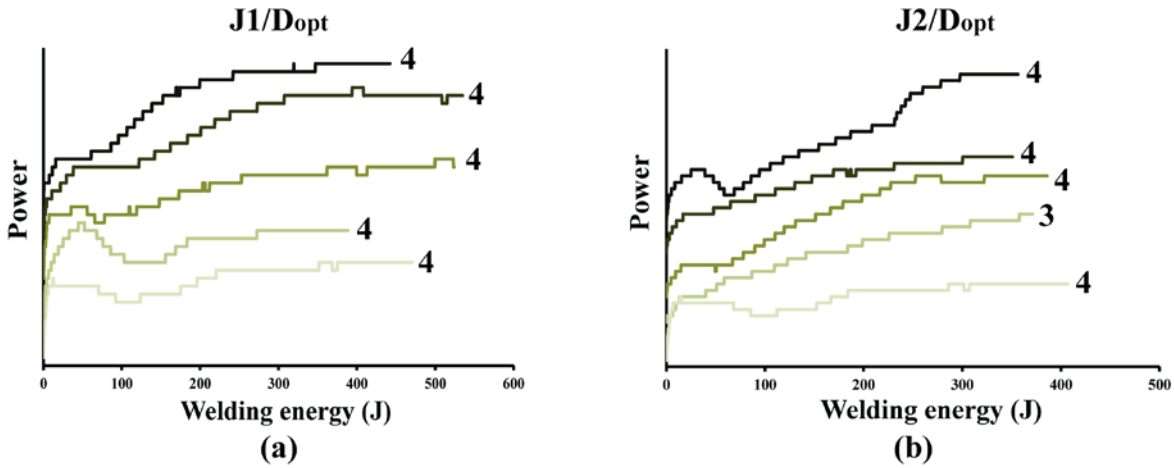

Fig. 9. Power curves for the optimum displacement-controlled SSW joints obtained in (a) Jig 1 (J1/D_{opt}) and (b) Jig 2 (J2/D_{opt}). The power curves are shifted vertically and the displacement curves are not shown here for clarity. The numbers correspond to the welding stages shown in Fig. 6.

3.2 Displacement ceiling

The reader should note that displacement-controlled welding of the SSW joints required the welding force to be continuously increased during the vibration phase of the welding process. Using a constant welding force, which is the common procedure used for displacement-controlled welding of full overlaps [2,3,4,14], was however found to result in a displacement plateau as shown in Fig. 12a, referred to as "displacement ceiling" hereafter. This displacement ceiling typically occurred before the optimum stage of the process, i.e. stage 4, was reached (Fig. 12a) which invalidated using displacement control as the welding strategy for the SSW joints.

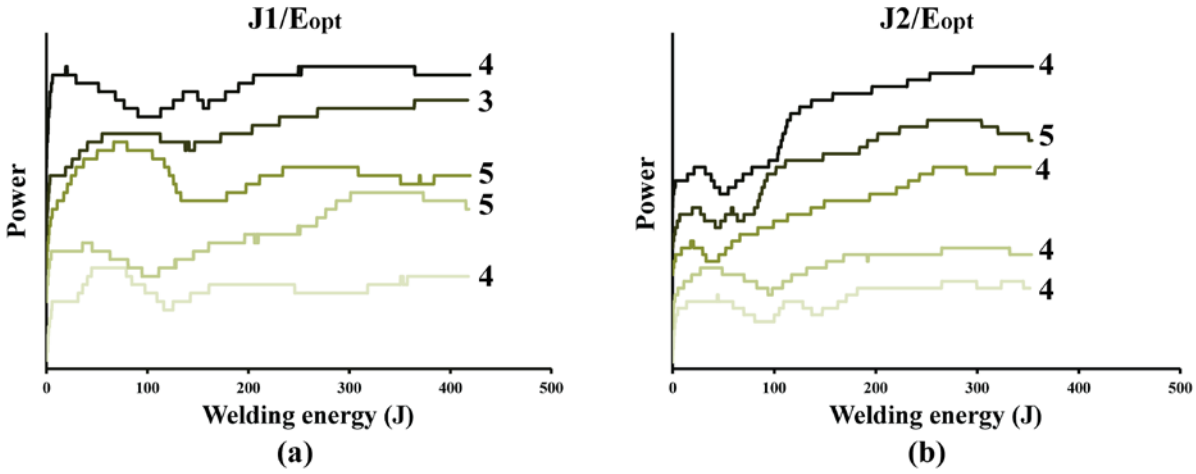

Fig. 10. Power curves for the optimum energy-controlled SSW joints obtained in (a) Jig 1 ($J1/E_{opt}$) and (b) Jig 2 ($J2/E_{opt}$). The curves are shifted vertically for clarity. The numbers correspond to the welding stages shown in Fig. 6.

The displacement ceiling was observed to occur in this study at around 0.10 mm for a constant welding force of 1500 N. Radial squeeze flow of the molten ED and hence gradual increase of the welded area was still observed within the displacement ceiling, despite the constant sonotrode displacement. The flow front,

which can be distinctly observed on the fracture surfaces in Fig. 7, was hence gradually pushed away from the original ED location and towards the colder adherends, which potentially caused it to solidify. The combination of solidified flow front together with the gradually decreasing welding pressure (owing to constant welding force over gradually increasing welding area) are believed to hinder the downward displacement of the sonotrode causing the displacement ceiling. By constantly increasing the welding force during the vibration phase, the solidified flow front could be further compressed resulting in a continuous increase of the sonotrode displacement which eventually enabled displacement-controlled welding of the SSW joints [15] (see Fig. 12b).

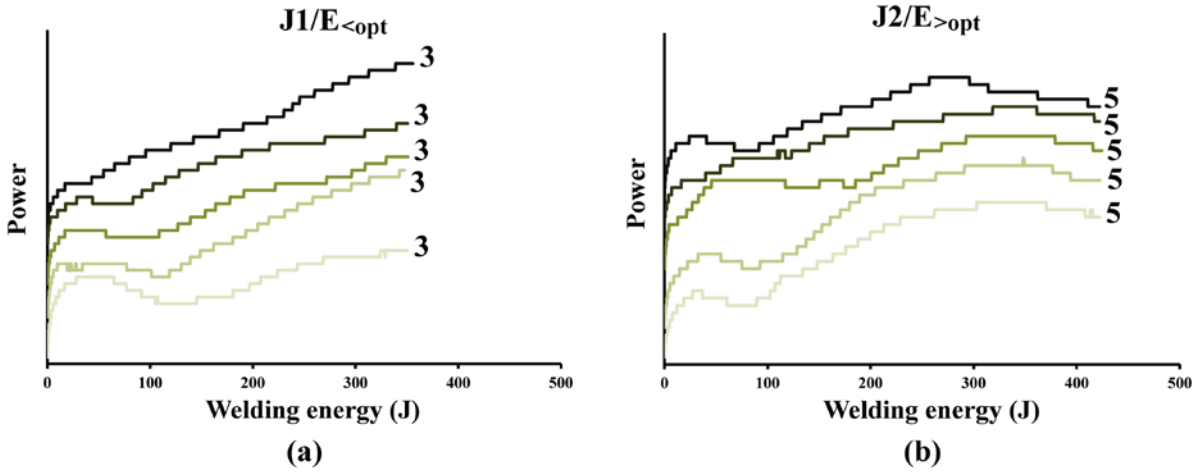

Fig. 11. Power curves for energy-controlled SSW joints obtained in: (a) Jig 1 at 350 J ($J1/E_{<opt}$), and (b) Jig 2 at 420 J ($J2/E_{>opt}$). The curves are shifted vertically for clarity. The numbers correspond to the welding stages shown in Fig. 6.

3.3 Weld strength and welded area

Table 2 and Fig. 13 show the ultimate failure load (UFL) and the final welded area (WA) of the SSW joints obtained under the optimum sets of conditions in Table 1.

It also shows the UFL and WA of two non-optimum cases, namely samples welded in Jig 1 at 350 J, i.e. below the optimum energy (SSW-J1/$E_{<opt}$), and samples welded in Jig 2 at 420 J, i.e. above the optimum energy (SSW-J2/$E_{>opt}$).

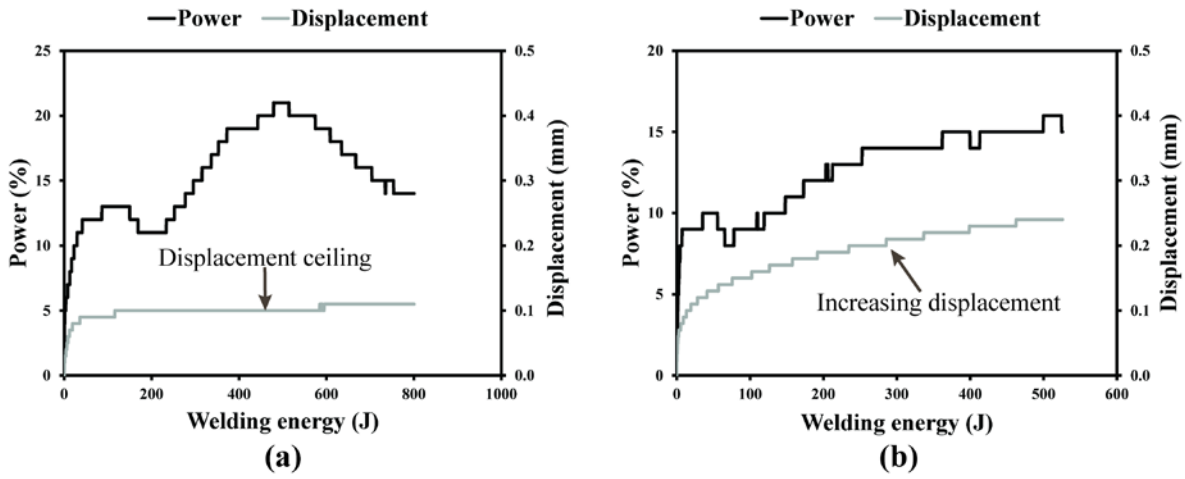

Fig. 12. Representative power curves for SSW joints obtained under (a) 1500 N constant welding force and (b) increasing welding force (1500 N initial force, 1000 N/s force ramp) (60.8 µm peak-to-peak amplitude).

The results shown in Table 2 and Fig. 13 indicate that, for each specific welding jig, the samples welded under optimum displacement (displacement-controlled welding) and under optimum energy (energy-controlled welding) conditions yielded similar UFL and WA values. It must be however noted that in general, the UFL and WA values obtained in Jig 2 were around 10% higher than those obtained in Jig 1. The relatively bigger WA and UFL in Jig 2 are believed to result from differences in the flow of the ED during the welding process in the different jigs. Fig. 14 shows a typical fracture surface of a SSW joint obtained in Jig 1 and one obtained in Jig 2. As seen in this Figure, welds performed in Jig 2 featured a somewhat radial ED flow (Fig. 14b), whereas the ED flow in Jig 1 showed a clear directionality (Fig. 14a). This is likely a

consequence of the less uniform strain state introduced in the ED by Jig1 which might as well have an impact on the extent of WA and hence, the UFL.

Table 2. UFL and WA values (average ± standard deviation) for the SSW joints studied in this research (COV: coefficient of variation).

Weld Reference	Ultimate Failure Load (N) (COV, %)	Welded Area, WA (mm^2) (COV, %)
SSW-J1/D_{opt}	3578.7 ± 162.3 (4.5)	95.4 ± 7.3 (7.6)
SSW-J1/E_{opt}	3834.1 ± 272.7 (7.1)	100.2 ± 9.1 (9.1)
SSW-J2/D_{opt}	3923.4 ± 242.5 (6.1)	109.7 ± 7.9 (7.2)
SSW-J2/E_{opt}	4240.8 ± 389.9 (9.2)	115.2 ± 12.0 (10.3)
SSW-J1/$E_{<opt}$	3149.8 ± 213.6 (6.8)	83.7 ± 4.2 (5.0)
SSW-J2/$E_{>opt}$	4132.8 ± 263.1 (6.4)	115.1 ± 8.6 (7.5)

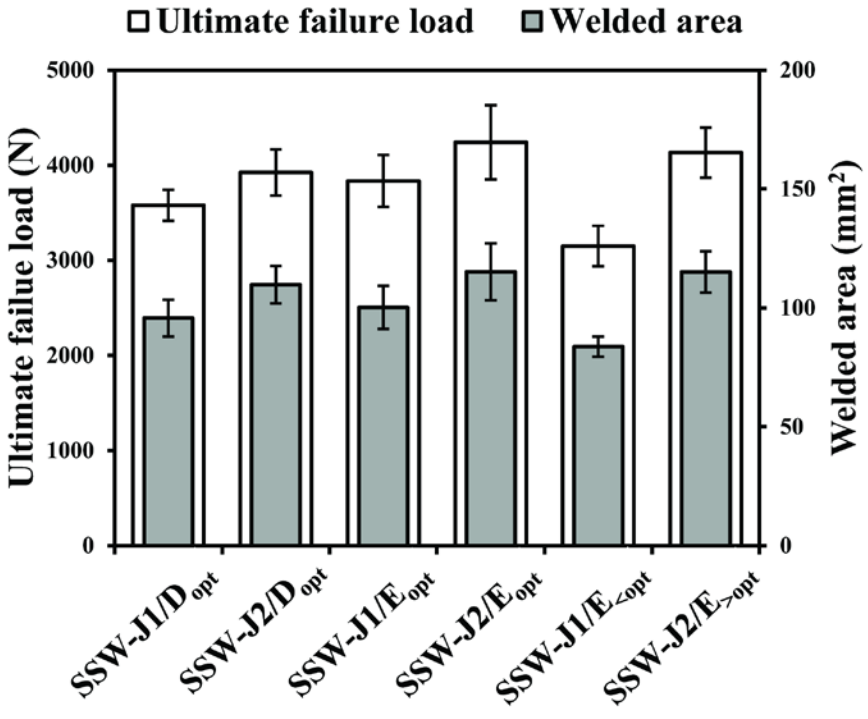

Fig. 13. UFL and WA of SSW joints manufactured with displacement-controlled and energy-controlled welding in combination with different clamping jigs.

Considering the samples welded in non-optimum conditions, the WA of the samples welded with a welding energy below the optimum was the smallest WA of all the welded samples produced in this study. This result is consistent with the fact that for these samples, the welding process did not reach the optimum stage, as seen in Fig. 11a. The UFL yielded by these samples was also the lowest one obtained in this study. The UFL and WA of samples welded with a welding energy above the optimum were however similar to those obtained with optimum energy.

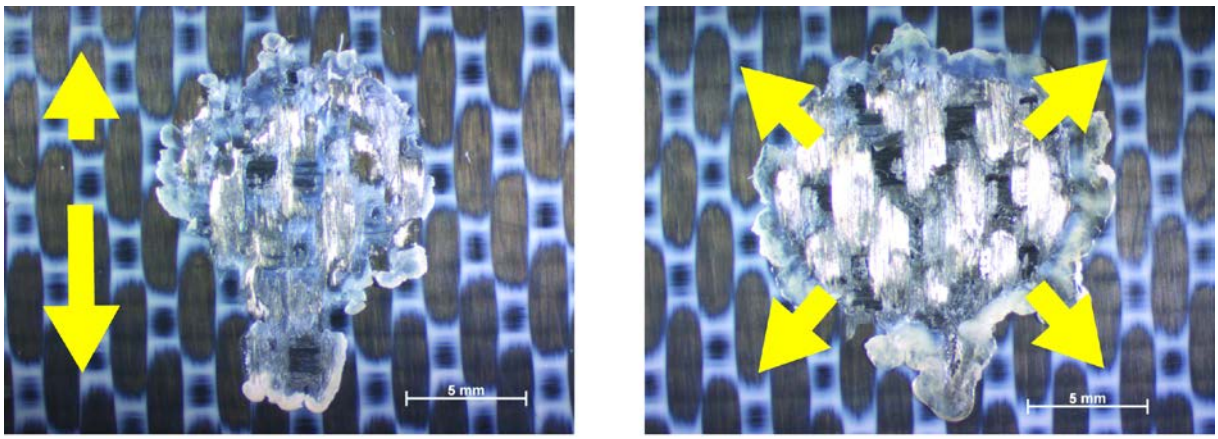

Fig. 14. Representative fracture surfaces of SSW joints welded in (a) Jig 1 and (b) Jig 2. The arrows indicate the non-uniform flow of the molten ED in Jig 1 and uniform flow of molten ED in Jig 2. (For interpretation of the references to colour in this figure legend, the reader is referred to the web version of this article.)

3.4 Failure modes

A fractographic analysis was carried out on the fracture surfaces of the SSW joints after mechanical testing. In displacement- and energy-controlled welds obtained with the optimum displacement and energy, respectively, fibre-matrix debonding was found to be the main failure mechanism, which is believed to indicate high weld

quality [16]. As shown in Fig. 15a and Fig. 15b, the main features on these fracture surfaces were bare fibres, deep fibre imprints on the matrix as well as torn fibres. Some of the samples, however, showed other secondary types of failure. One of these secondary failure types was characterized by resin-rich fracture surfaces with partially debonded fibres, shallow fibre imprints and fractured resin (Fig. 16a). The other secondary failure type showed porosity and significant fibre distortion together with the predominant bare fibres and deep fibre imprints as illustrated in Fig. 16b. The resin-rich fracture surfaces (Fig. 16a) are believed to correspond to under-welded samples, i.e. those cases where the vibration was stopped before the optimum welding stage was reached (namely occasional samples welded in stage 3, see Fig. 10a). Whereas the fracture surfaces with porosity (Fig. 16b) are believed to correspond to over-welded samples, i.e. those cases where the vibration was stopped beyond the optimum welding stage (namely occasional samples welded in stage 5, see Fig. 10a). These secondary failure types, mostly observed in samples welded in energy control-mode, indicate that the same optimum energy can lead to varying weld quality. This relates to the fact that the welding energy is not only invested in creating the welded joint but is also dissipated in the adherends, the welding fixture and the base [13]. Hence the exact energy used to create the weld is unpredictable and scatter in weld quality resulting from energy-controlled welding is unavoidable.

Regarding the samples welded in non-optimum conditions, resin-rich failure, with the same features as those shown in Fig. 16a, was invariably found for samples welded at 350 J in Jig 1, i.e. at an energy value below the optimum. This resin-rich failure is consistent with the smaller welded area and hence thicker weld lines (for the

same ED volume). In contrast, samples welded at 420 J in Jig 2, i.e. at an energy value above the optimum, mostly showed fracture surfaces with obvious porosity and fibre distortion, similar to that shown in Fig. 16b.

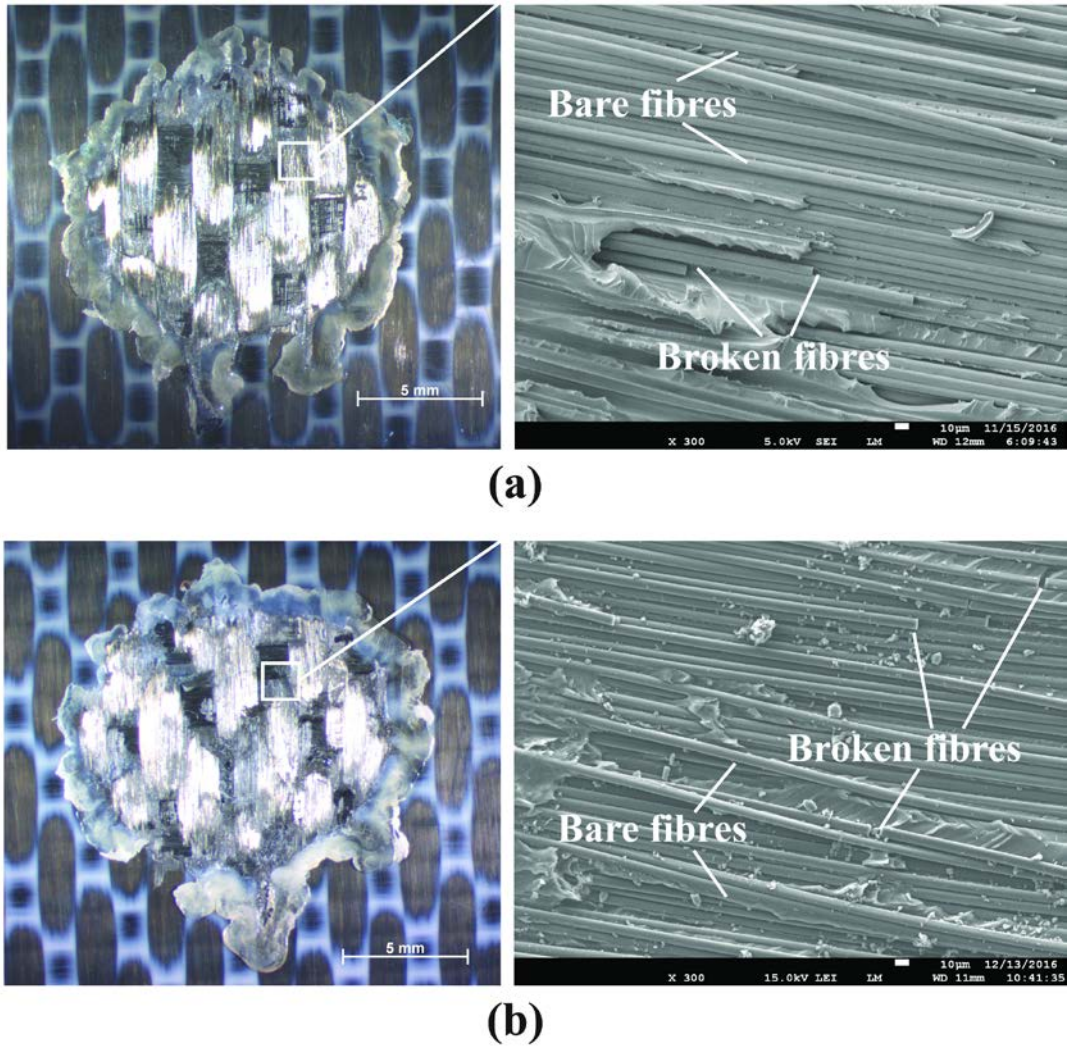

Fig. 15. Representative fracture surfaces (left) and SEM detail (right) of SSW joints welded at (a) the optimum displacement (displacement-controlled welding) and (b) the optimum energy (energy-controlled welding).The scale bars are 5 mm (for stereo-microscopy) and 10 µm (for SEM). Both samples were welded in Jig 2. (For interpretation of the references to colour in this figure legend, the reader is referred to the web version of this article.)

4 DSW joints: results and discussion

4.1 Sequential welding process

One of the main questions arising in sequential welding concerns possible interactions between the different welding processes, in this case welding of the first and of the second spot, performed in the same overlap.

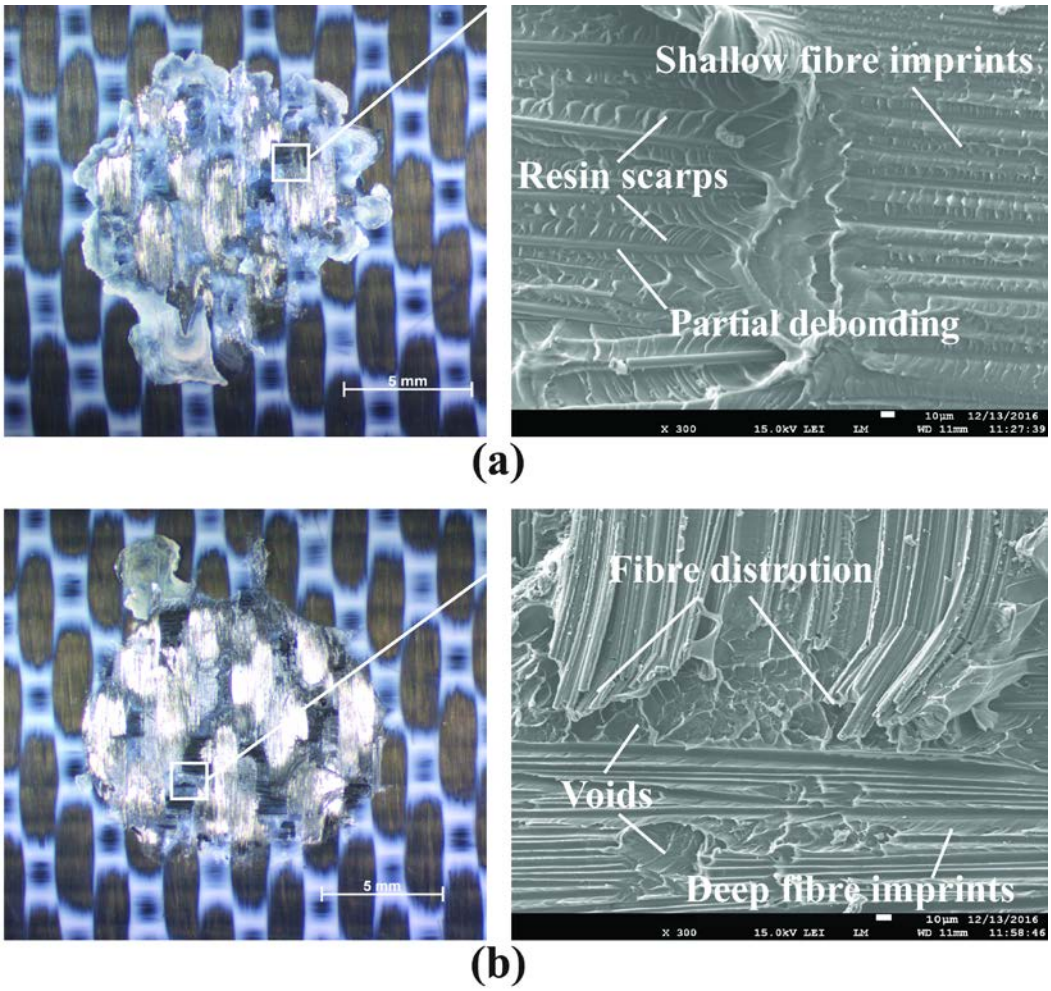

Fig. 16. Fracture surfaces (left) and SEM details (right) showing secondary failure types in SSW joints welded at the optimum energy in (a) Jig 1 and (b) Jig 2. The SEM micrograph in (a) shows significant presence of resin scarps and cusps, indicating failure took place in the thermoplastic resin [17]. In contrast, void imprints combined with deep laminate tearing and fibre distortion are found in the SEM micrograph in (b). The scale bars are 5 mm (for stereo-microscopy) and 10 µm (for SEM). (For interpretation of the references to colour in this figure legend, the reader is referred to the web version of this article.)

Firstly, potential interactions between the first welding process, i.e. welding of the first spot, and the pristine second ED could be partial melting of the latter or hindered downward displacement during the former. Fig. 17 shows the fracture surfaces of a DSW joint interrupted after only welding of the first spot. As seen in this Figure, the second ED did not show any signs of melting after welding of the first spot, only those attributable to the fixing of the ED on the adherend with the handheld welder prior to the welding process. This can be explained by the fact that the small-size sonotrode only covered the first ED during welding of the first spot. Most of the welding force and vibration were then applied on the first ED leading to preferential heat generation at that location. Owing to the stiff nature of the composite adherends, part of the force and vibration were also transmitted to the second ED, however they were not high enough to cause melting.

Moreover, inspection of the welding curves of the DSW joints (see Fig. 18) indicated that the presence of the pristine second ED did not hinder the downward displacement of the top adherend during welding of the first spot as the displacement curves for both spots had similar increasing trends and also similar to the SSW joints. This was probably enabled by the small thickness of the EDs and the flexibility of the adherends.

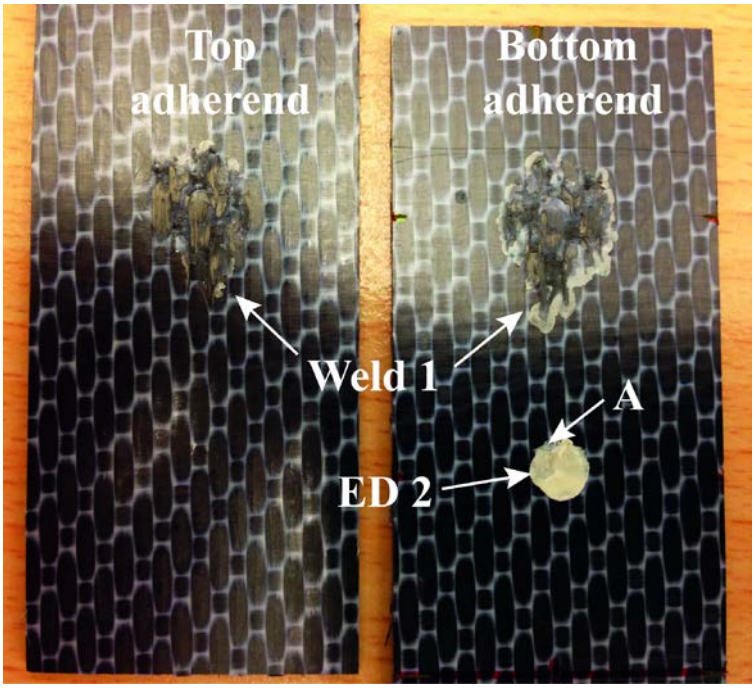

Fig. 17. Fracture surfaces of a DSW joint after only welding the first spot. A: local melt of the ED caused by fixing to the adherend with handheld welder prior to welding process.

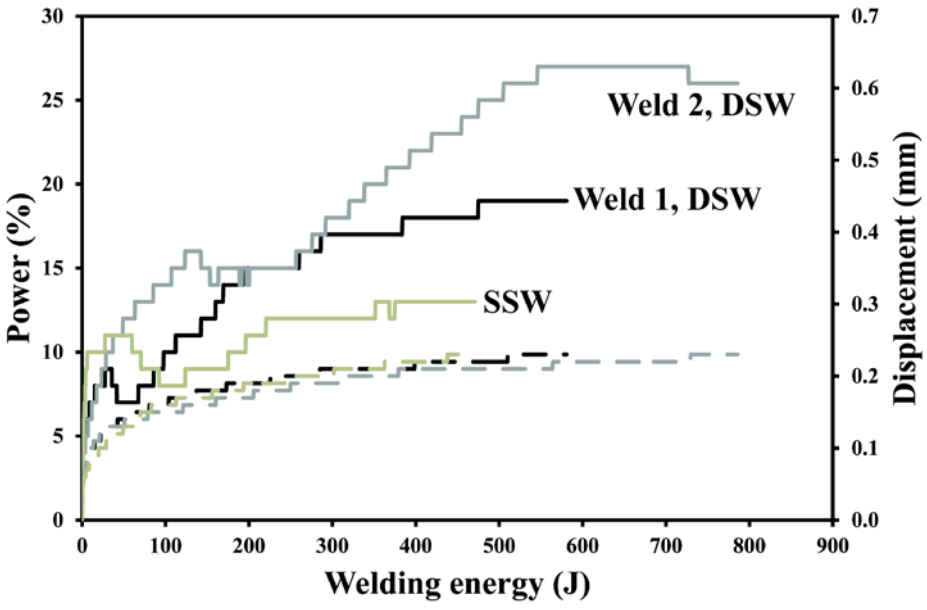

Fig. 18. Representative power (solid line) and displacement (dashed line) curves for both welded spots in a DSW joint and for a SSW joint produced using displacement-controlled welding at optimum displacement (0.23 mm), 60.8 µm peak-to-peak amplitude, 1500 N welding force and 1000 N/s increasing force during the vibration phase (welding jig J1).

Secondly, potential interactions between the second welding process, i.e. welding of the second spot, and the already welded first spot could be an increased misalignment, i.e. loss of parallelism, between the adherends and a change in the energy needed to weld the second spot with optimum quality. As seen before (section 3.3), misalignment between the adherends can be expected to have an impact on the welded area. As it will be shown in section 4.2, no significant differences were however found between the welded area of the first and the second spot in the DSW joints, provided that both spots were welded in optimum conditions. Nevertheless, the already welded first spot did cause an increase on the average energy needed to weld the second spot (for a certain fixed displacement), as illustrated in Fig. 18.

4.2 Weld strength, welded area and failure analysis

Table 3 and Fig. 19 show the UFL (ultimate failure load) and final welded area (WA) of the DSW joints obtained in optimum displacement conditions (D_{opt}=0.23 mm, displacement-controlled welding), DSW-J1/D_{opt}, and the double-spot welded joints obtained in optimum energy conditions (E_{opt}=420 J, energy-controlled welding), DSW-J1/E_{opt}. As a reference, the UFL and WA and values of the SSW-J1/D_{opt} and of the SSW-J1/E_{opt} samples are also included in Table 3 and Fig. 19.

As seen in Table 3 and Fig. 19, the DSW-J1/E_{opt} joints showed smaller total welded area (around 20% smaller) than the DSW-J1/D_{opt} joints. Likewise, the average UFL of the DSW-J1/E_{opt} joints was approximately 20% lower than that of the DSW-J1/D_{opt} joints. The scatter of the UFL values for the DSW-J1/E_{opt} joints was also relatively high (above 10%).

The analysis of the welded area of each individual spot in the DSW-J1/D_{opt} and the DSW-J1/E_{opt} joints provided the results shown in Fig. 20. As seen in this Figure, the two spots in the DSW-J1/D_{opt} joints had similar average welded areas, which in turn were similar to the reference WA in SSW-J1/D_{opt} joints. In the case of the DSW-J1/E_{opt} joints the spots welded in the first place were slightly smaller than the ones in the reference SSW-J1/E_{opt} joints. This probably indicates that the optimum energy to produce the SSW joints (also used for the DSW joints) is not necessarily the optimum energy to produce the first spot in the DSW joints owing to differences in adherend and overlap size between the two cases. More importantly, the spots welded in second place in the DSW-J1/E_{opt} joints were approximately 20% smaller than the ones welded in first place, evidencing that the welding energy used was well below the energy needed to produce optimum welds. These results are consistent with those shown in Fig. 18. For the specific DSW and SSW joints considered in that Figure, the first spot in the DSW joint required approximately 25% higher energy to reach the optimum displacement than the spot in the SSW joint. In the case of the second spot in the DSW joint, the welding energy required to reach optimum displacement was approximately 65% higher than that of the SSW joint.

Table 3. UFL and WA values (average ± standard deviation) for both DSW-J1 and SSW-J1 joints studied in this research (COV: for coefficient of variation). The welded area of the DSW-J1 joints was calculated as the sum of the welded areas of the two individual spots.

Weld Reference	Ultimate Failure Load (N) (COV, %)	Welded Area (mm^2) (COV, %)
DSW-J1/D_{opt}	7037.5 ± 467.8 (6.6)	196.3 ± 14.3 (7.3)
DSW-J1/E_{opt}	5838.3 ± 780.0 (13.3)	160.2 ± 8.9 (5.5)
SSW-J1/D_{opt}	3578.7 ± 162.3 (4.5)	95.4 ± 7.3 (7.6)
SSW-J1/E_{opt}	3834.1 ± 272.7 (7.1)	100.2 ± 9.1 (9.1)

Finally, fractographic analysis of the welded samples after testing showed that the two welds in the DSW-J1/D_{opt} joints featured bare fibres, deep fibre imprints on the matrix as well as torn fibres (see Fig. 21), characteristic of optimum welded joints. In the case of the DSW-J1/Eopt joints, the second welded joint featured resin-rich fracture surfaces with partially debonded fibres, shallow fibre imprints and fractured resin (see Fig. 22), characteristic of welded joints obtained at a welding energy below the optimum.

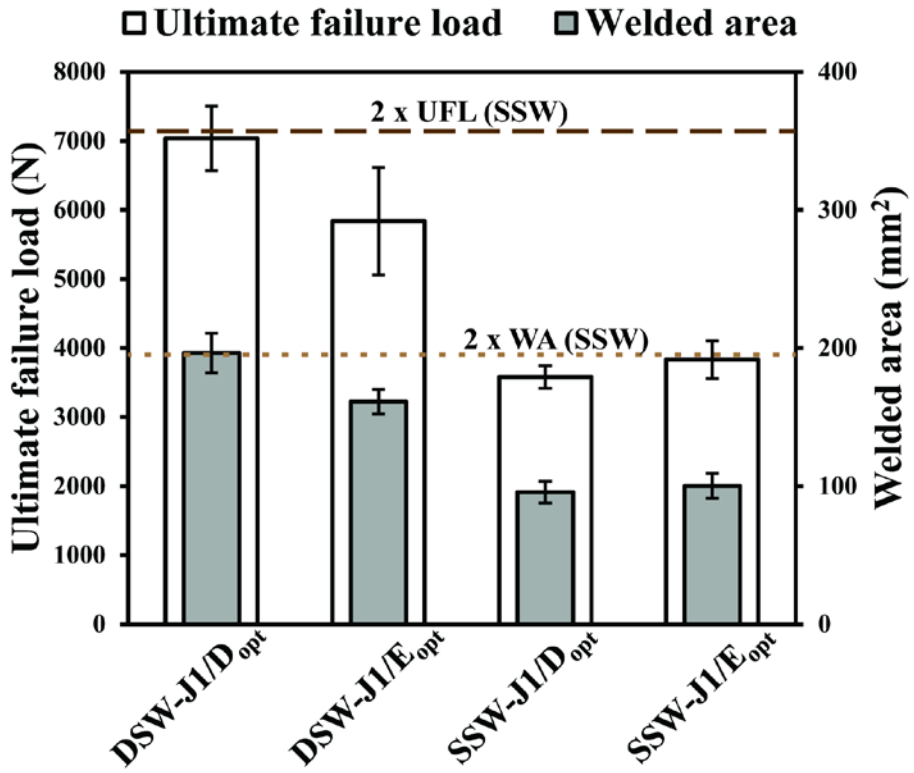

Fig. 19. UFL and WA of the DSW-J1 and the SSW-J1 joints manufactured with displacement- and energy-controlled welding (D_{opt}=0.23 mm, E_{opt}= 420 J), 60.8 µm peak-to-peak amplitude, 1500 N welding force and 1000 N/s increasing force during the vibration phase. The dotted and dashed lines show two times the average WA and UFL (SSW-J1/D_{opt} and SSW-J1/E_{opt}), respectivley, as indicative reference values.

The results presented in this section and in sections 3.1, 3.3 and 4.1, indicate that after the first spot was welded in the DSW-J1/E_{opt} joints, it introduced an additional constraint to the relative movement of the adherends and consequently, the initial welding energy was not high enough to produce optimum welds. As a result, the load-carrying capability of the DSW joints obtained under a constant welding energy was penalised. Contrarily, the same displacement value led to both welded spots with optimum quality in the DSW-J1/D_{opt} joints.

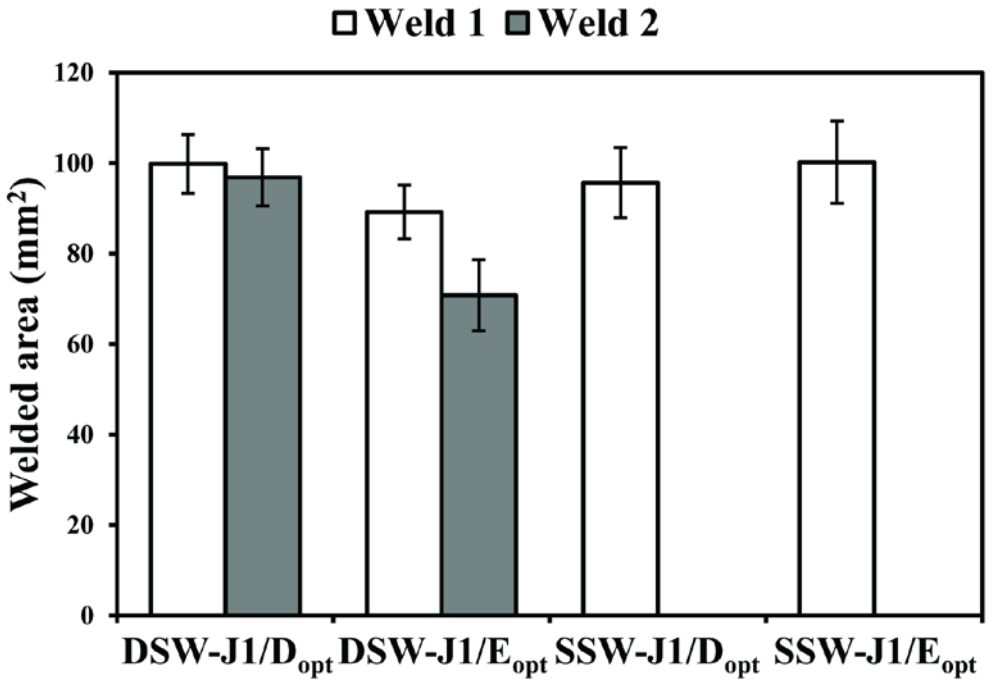

Fig. 20. Welded area of individual spots in both DSW-J1/D_{opt}, DSW-J1/E_{opt}, SSW-J1/D_{opt} and SSW-J1/E_{opt} joints.

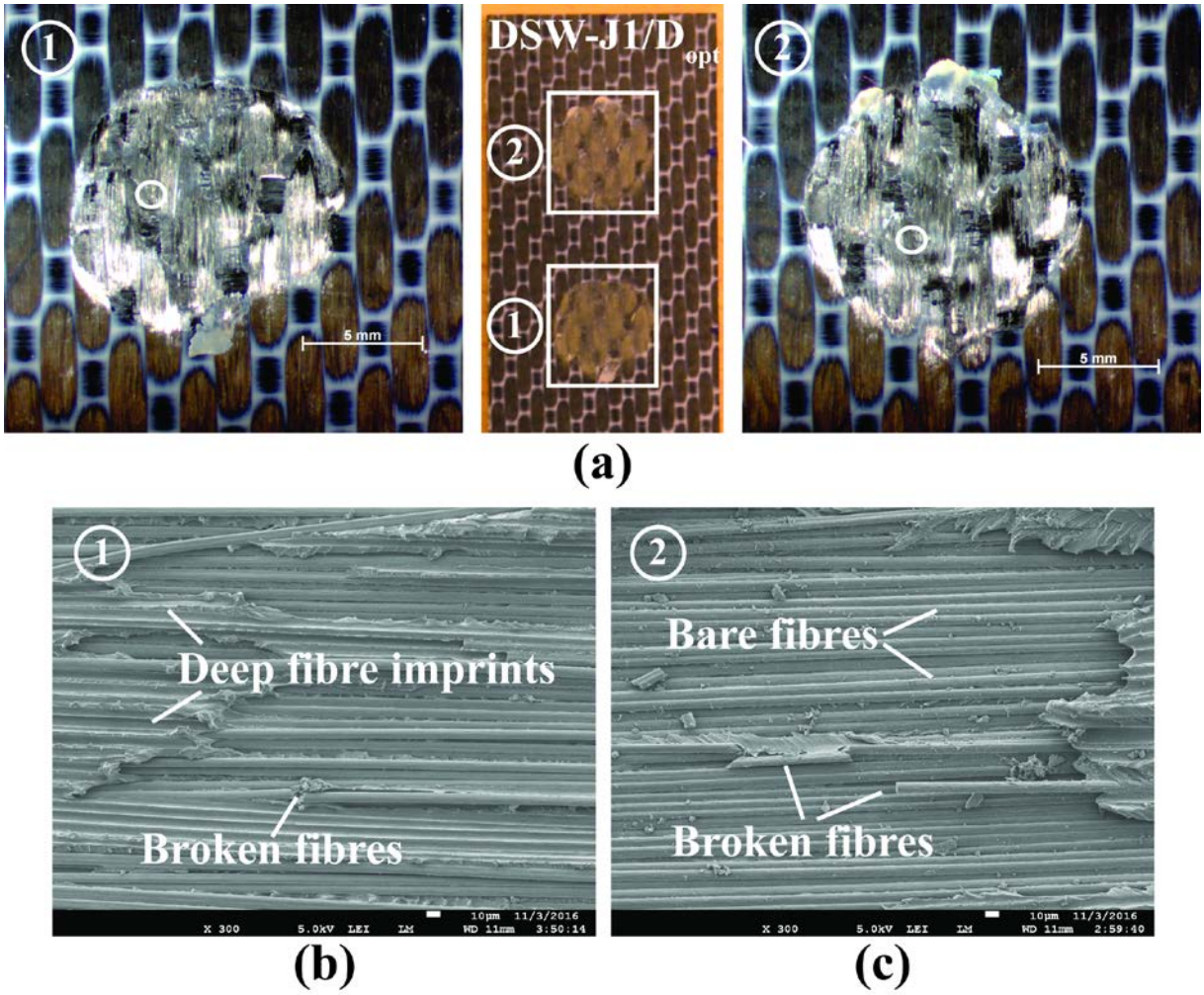

Fig. 21. (a) Representative fracture surfaces of the DSW-J1/D_{opt} joints. The numbers indicate the welding sequence (Fig. 5). SEM micrographs (b) and (c) show the details of the areas circled in the fracture surfaces of Weld 1 and Weld 2, respectively. The scale bars are 5 mm (for stereo microscopy) and 10 µm (for SEM).

5 Conclusions

In this paper, a series of experimental studies were carried out to test the following hypothesis: the changes introduced in the boundary conditions by each new welded spot in sequential ultrasonic welding of multi-spot welded joints affect the welding energy required to obtain optimum weld quality, but do not affect the displacement required to obtain optimum weld quality in displacement-controlled

welding. To this end, the effect of boundary conditions in single-spot displacement-controlled and energy-controlled welds was investigated. Subsequently, sequential welding of double-spot welded joints under displacement-control and energy-control welding modes was investigated. The main conclusions obtained from this research are the following:

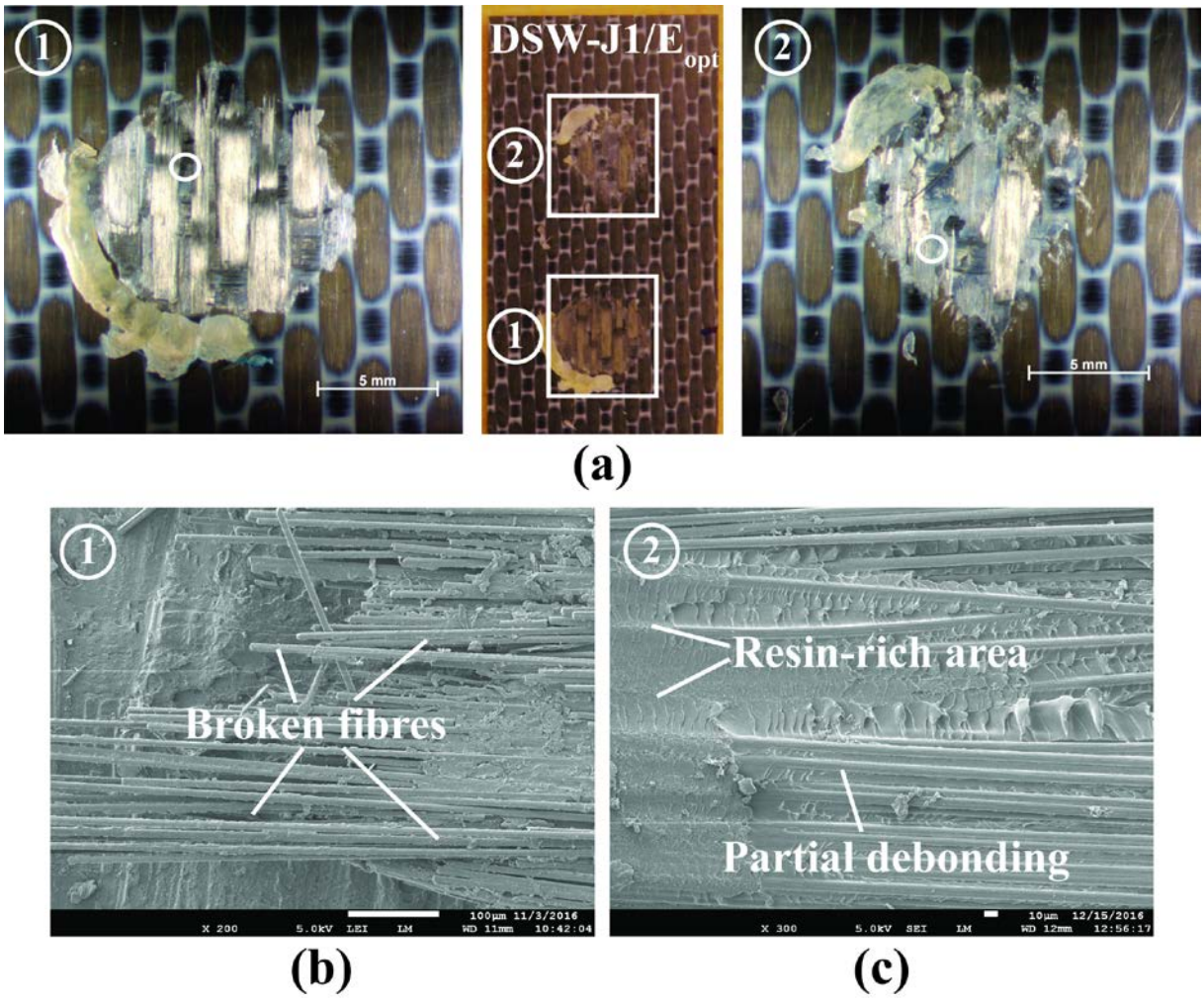

Fig. 22. (a) Representative fracture surfaces of the DSW-J1/E_{opt} joints. The numbers indicate the welding sequence (Fig. 5). SEM micrographs (b) and (c) show the details of the areas circled in the fracture surfaces of Weld 1 and Weld 2, respectively. The scale bars are 5 mm (for stero microscopy) and 10 µm (for SEM).

- Changes in boundary conditions, in particular the use of different welding jigs, were found to have a significant impact on the welding energy required to obtain

single-spot welded joints with optimum quality. In particular, higher constraints imposed into the movement of the adherends resulted in higher welding energy requirements. Contrarily, the displacement required to obtain optimum welded joints in displacement-controlled welding was found to be virtually insensitive to the said changes.

- In sequential welding of double-spot welded joints, the most significant interaction between the two welding processes occurring in the same overlap was the fact that welding of the first spot affected the energy needed for an optimum second spot. Specifically, as a consequence of the constraints added to the relative movement between adherends by the first spot, an energy increase was necessary to obtain an optimum second spot. Using a constant welding energy for the two spots was found to decrease in the total amount of welded area and consequently to decrease the load-carrying capability of the joints. Contrarily, the same displacement value resulted in optimum quality spots in displacement-controlled welding of double-spot welded joints and hence no penalty to their load-carrying capability.
- In order to successfully perform displacement-controlled spot welding operations the welding force had to be gradually increased during the vibration phase of the welding process to prevent the displacement from levelling off into a displacement ceiling.

As a summary, these conclusions indicate that displacement-controlled ultrasonic welding has the unique potential to enable sequential welding of multi-spot

joints with uniform high-quality based on a fixed set of welding parameters, i.e. avoiding recalculation of the welding parameters for each individual spot.

Acknowledgements

T. Zhao thanks the PhD Scholarship Fund from the China Scholarship Council (CSC) for overseas study. Part of the work presented in this paper was performed in the framework of the TAPAS 2 project, subsidized by the Ministry of Economic Affairs in the Netherlands. Some of the results in this paper were presented at the ICCM21 Conference held in Xi'an, China, in August 20th -25th 2017.

References

[1] Ageorges C, Ye L, Hou M. Advances in fusion bonding techniques for joining thermoplastic matrix composites a review. Compos Part A: Appl Sci Manuf 2001;32:839-857.
[2] Villegas IF. Strength development versus process data in ultrasonic welding of thermoplastic composites with flat energy directors and its application to the definition of optimum processing parameters. Compos Part A: Appl Sci Manuf 2014;65:27-37.
[3] Villegas IF. In situ monitoring of ultrasonic welding of thermoplastic composites through power and displacement data. J Thermoplast Compos Mater 2013;28(1):66-85.
[4] Palardy G, Villegas IF. On the effect of flat energy directors thickness on heat generation during ultrasonic welding of thermoplastic composites. Compos Interfaces 2016;24(2):203-214.
[5] Zhao T, Palardy G, Villegas IF, Rans C, Martinez M, Benedictus R. Mechanical behaviour of thermoplastic composites spot-welded and mechanically fastened joints: A preliminary comparison. Compos Part B: Eng 2016;112:224-234.
[6] Patel VK, Bhole SD, Chen DL. Ultrasonic spot welding of lightweight alloys. In: Proceedings of 13th International Conference on Fracture. Beijing, June, 2013. p.1-10.
[7] Macwan A, Patel VK, Jiang XQ, Li C, Bhole SD, Chen DL. Ultrasonic spot welding of Al/Mg/Al tri-layered clad sheets. Mater Des 2014;62:344-351.
[8] Zhou B, Thouless MD, Ward SM. Predicting the failure of ultrasonic spot welds by pull-out from sheet metal. Int J Solids Struct 2006;43:7482–7500.
[9] Patel VK, Bhole SD, Chen DL. Microstructure and mechanical properties of dissimilar welded Mg–Al joints by ultrasonic spot welding technique. Sci Technol Weld Joining 2012;17(3):202-206.
[10] Lu HM, Benatar A. Sequential ultrasonic welding of PEEK/Graphite composite parts. In: Proceedings of the Annual Technical Conference ANTEC. Montreal, 1991. p.2523-2526.

[11]Harras B, Cole KC, Vu-Kanh T. Optimization of USW of PEEK-carbon composites. J Reinf Plast Compos 1996;15:174-182.
[12]General Dynamics/Convair Division. Graphite composite truss welding and cap section forming subsystem. Volume II: progam results, final report. NASA-CR-160932. 1980.
[13]Benatar A, Gutowski TG. Ultrasonic Welding of PEEK Graphite APC-2 Composites. Polym Eng Sci 1989;29(23):1705-1721.
[14]Villegas IF, Grande BV, Bersee HEN, Benedictus R. A comparative evaluation between flat and traditional energy directors for ultrasonic welding of CF/PPS thermoplastic composites. Compos Interfaces 2015;22(8):717-729.
[15]Broek CA. Optimising Ultrasonic Welding of Carbon Fibre PEKK Composites by investigating integrated energy directors, displacement ceilings and displacement-controlled welding strategies. Master thesis, 2015.
[16]Villegas IF, Bersee HEN. Ultrasonic welding of advanced thermoplastic composites: An investigation on energy-directing surfaces. Adv Polym Tech 2010;29(2):112-121.
[17]Greenhalgh ES. Failure Analysis and Fractography of Polymer Composites. Woodhead Publishing in Materials; 2009.